

Electron Attachment Induced Shape Resonances in AT Base Pairs

Sneha Arora^a, Jishnu Narayanan S J^a and Achintya Kumar Dutta^{a*}

^a*Department of Chemistry, Indian Institute of Technology Bombay, Powai, Mumbai 400076, India.*

Abstract

In this study, we examined the influence of base pairing and π - π stacking interactions on electron attachment induced resonances in adenine-thymine base pair. Resonance positions and widths were computed using the DLPNO based equation of motion coupled-cluster method combined with the Padé approach. We identified seven π^* shape resonances in both linear and stacked AT geometries, consistent with the total number found for isolated adenine and thymine. Natural orbital analysis shows that low energy resonances exhibit more electron density delocalized over both nucleobases. This delocalization is more pronounced in the stacked AT geometry and leads to significant stabilization of the resonance states.

1. Introduction

The study of electron interactions with biomolecules, particularly DNA, has gained considerable attention in recent decades due to the crucial role these interactions play in radiation effects and their biological implications.¹ When ionizing radiation such as X-rays or γ -rays interacts with biomolecules, it produces secondary electrons (SEs)²⁻⁵ along with other products.^{2,6-10} These electrons play an important role in radiative cellular damage, including mutations, disruption of genomic stability, and apoptosis.^{2-5,11} The energy distribution of SEs produced by ionizing radiation typically peaks around 9 eV,¹² with the majority of electrons having energies below 20 eV.^{3,13-17} These SEs generate low energy electrons (LEEs) through a series of successive inelastic collisions, resulting in a spectrum that peaks below 1 eV with a half-width at half-maximum of ~ 2 eV.¹³⁻¹⁹ Previous studies have shown that LEEs with energies below the ionization threshold of DNA (~ 7.5 -10 eV)^{20,21} have the potential to cause significant molecular damage to DNA. Woldhuis et al.²² and Boudaïffa et al.²³ are among the first to demonstrate that low energy electrons can directly interact with DNA in aqueous environments, inducing both single and double strand breaks.

LEE interaction with biomolecules leads to the formation of excited transient negative ions (TNI*) or resonances with lifetimes ranging from 10^{-12} to 10^{-15} seconds.²⁴ These species may undergo autodetachment, relax to the ground state radical anion, or dissociate via dissociative electron attachment (DEA)²⁵⁻²⁸ which results in bond breaking.^{23,29-37} Resonance states play an important role across a wide range of scientific and technological domains, from high energy processes such as plasma dynamics, attosecond and X-ray spectroscopies,^{38,39} to low energy electron-molecule interactions relevant to interstellar chemistry, LEE induced radiation damage to biomolecules. These are generally classified as either one-particle (1p) or two-particle-one-hole (2p1h) states, based on the electronic configuration of the neutral target prior to electron attachment.^{35,36,40-45} One-particle resonance, also called a shape resonance, is formed when an incoming electron gets temporarily trapped in the interaction potential with a neutral molecule. The shape of the potential is formed by the combined effects of the attractive polarization potential and the repulsive centrifugal potential.⁴⁶ However, electron attachment to an excited state leads to a 2p1h resonance state which is characterized by a hole in one of the occupied molecular orbitals.³⁵

Resonance states are non-stationary, finite lifetime states that couple to the continuum and involve a superposition of multiple configurations.⁴⁷⁻⁵⁶ These states are characterized by Siegert energies, $E_{res} = E_R - i\Gamma/2$, where the real part denotes the resonance energy and the imaginary part is related to the inverse lifetime.⁴⁷ They exhibit bound state like behavior near the interaction region but possess an outgoing oscillatory tail outside the potential barrier. As a result, the corresponding wavefunction is non-square integrable. Hence, conventional methods employed for bound state electronic structure calculations are unsuitable for describing resonance states, and one needs to use special techniques to study these kinds of states. The development of so-called “ L^2 ” *ab initio* quantum chemical methods, such as complex scaling (CS),⁴⁸⁻⁵² complex absorbing potentials (CAP),⁵²⁻⁶⁰ and stabilization approach,⁶¹⁻⁶⁴ has significantly advanced the theoretical treatment of resonances in many electron systems. Among these methods, the stabilization approach in which conventional quantum mechanical techniques can be used without any modification stands out as one of the straightforward methods for computing resonances in quantum chemistry.⁶¹⁻⁶⁴

Electron attachment induced resonances of isolated DNA/RNA bases have been the subject of extensive study from both theoretical and experimental perspectives.^{34-36,42,45,65-75} Scattering techniques have been used to identify resonances in nucleobases, nucleosides, and nucleotides, mostly using DFT as the method of calculation.¹⁹ Accurate electron correlation methods were also used for resonance calculations. The shape resonances of nucleobases were reported using the complex absorbing potential method combined with symmetry adapted cluster configuration interaction (SAC-CI). The orbital stabilization method has also been applied to uracil within a DFT framework using Koopmans’ theorem.⁵³ We have recently demonstrated that TD-DFT method can provide a low-cost way to simulate resonances of nucleobases,⁷⁶ if proper exchange-correlation functionals are used. Matsika and co-workers has combined orbital stabilization technique with EOM-EA-CCSD and XMCQDPT2 method to predict both shape and core-excited resonances in DNA and RNA nucleobases.^{35,77,78}

Most previous theoretical studies of anionic resonances in genetic material have used nucleobases as model systems for DNA. Recent studies have shown that aqueous and amino acid environments can significantly affect nucleobase resonances.^{74,79} However, since most genetic materials are double stranded, studying excess electron interactions with hydrogen bonded base pairs is necessary. Therefore, base pairs serve as fundamental model systems of DNA, making them essential for investigating electron attachment processes. Since they

capture the key electronic interactions present in the genetic material, studying base pairs provides direct insight into how low energy electrons interact with and potentially damage DNA. Sevilla and co-workers⁸⁰ conducted the first *ab-initio* investigation of electron attached states in DNA base pairs at the Hartree-Fock level.¹³² Their work on adenine-thymine (AT) and guanine-cytosine (GC) pairs revealed that electron attachment generates valence-type radical anions capable of inducing inter base proton transfer. Adamowicz and co-workers⁸¹ reported a negative adiabatic electron attachment energy (-0.40 eV) for the AT base pair at the MP2/6-31+G(d,p) level, indicating unfavorable electron attachment. In contrast, their MP2/6-31++G** study on the GC base pair revealed the coexistence of dipole-bound and valence-bound anionic states, with the excess electron localized on the cytosine in both cases.⁸² It has been demonstrated that the interconversion between valence and dipole-bound states happens in base-pairs through mixing electronic and nuclear degrees of freedom, and the dipole-bound state can act as a doorway for the capture of low-energy electrons. The AT base pair provides a particularly interesting test case as it has a low dipole moment and does not support any dipole-bound state. The resonance states would be the dominant pathway for electron attachment. This study aims to investigate the nature of electron attachment-induced resonances in AT base pairs.

2. Computational details:

The neutral geometries of nucleobases and base pairs are optimized at the RI-MP2^{83,84} level of theory with def2-TZVP basis.⁸⁵ Further, several different conformers of Adenine-Thymine base pair (stacked and linear) are generated using CREST.⁸⁶ The lowest energy conformer for stacked and linear AT is selected and re-optimized at the RI-MP2/def2-TZVP level of theory for subsequent computations. Single-point electron attachment energies are evaluated using the EA-EOM-DLPNO-CCSD^{87,88} method with the NORMALPNO setting. The EA-EOM-DLPNO-CCSD states are primarily characterized by the single-excitation (R1) component, with singles amplitudes consistently exceeding 90%. Resonance stabilization curves are obtained by scaling the diffuse functions of the augmented cc-pVDZ basis set,⁸⁹ achieved by adding one additional diffuse function of 2s, 2p, and 2d angular momentum type to all heavy atoms present in the molecule.⁷¹ Their work suggests that when augmenting a basis set with additional diffuse functions, the exponent of each added diffuse function is usually chosen to be half the value of the smallest (most diffuse) exponent already present for that atom. By dividing the gaussian exponents by a real factor (α), the additional diffuse functions are

scaled. The expanded basis set is denoted by the notation cc-pVDZ+2s2p2d. The relevant auxiliary basis set was selected using Autoaux⁹⁰ tool of ORCA 5.0.3 software.^{91,92} The optimized structures of AT base (stacked and linear) base pairs are provided in the Supplementary information. (Figure S1)

The comprehensive stabilization graph for thymine, plotted using the EA-EOM-DLPNO-CCSD method, is presented in Figure 1, showcasing the dependence of energy on the scaling parameter α . Resonance wave functions behave like localized states near the interaction region and are largely unaffected by small variations in basis set scaling. Consequently, in a stabilization graph, resonance states appear as stable energy regions with respect to the scaling parameter α , whereas continuum states display significant energy fluctuations as α varies. The resonance via padé (RVP) method is then employed to compute the resonance position and width based on the stable portion of the stabilization plot.⁶² The calculations using the RVP method are performed using open-source software known as "Automatic RVP."⁹³

The molecular systems investigated include thymine, adenine, and their base pairs in various configurations. Throughout this work, the following notations are employed as T (thymine), A (adenine), AT (adenine-thymine base pair), sAA (stacked adenine-adenine base pair), sTT (stacked thymine-thymine base pair) and sAT (stacked adenine-thymine base pair).

4. Result and discussion:

In the study we keep our attention only on shape resonances. To understand the effect of base-pairing on the position and width of shape resonances, one needs to first investigate the shape resonances of the individual base pairs. It also helps one to gauge the accuracy of the theoretical model used for the simulation as accurate theoretical results already available for individual bases.^{34–36,42,45,65–75,94}

4.1 Thymine shape resonances:

The shape resonance states of Thymine were experimentally investigated using low-energy electron transmission spectra (ETS) experiments.⁹⁵ Three resonance states were detected, and the states are blue shifted upwards compared to uracil by approximately 0.07, 0.13, and 0.22 eV. This blueshift can be attributed to the σ -electron donating nature of the C5 methyl group present in thymine.⁹⁵

In this work, we have identified three low-lying shape resonances thymine anion using the EA-EOM-DLPNO-CCSD method combined with the RVP approach. These states are termed as $1\pi^*$, $2\pi^*$, and $3\pi^*$ resonances in the order of increasing energy. Figure 1A illustrates the energy stabilization diagram for thymine anion, along with the corresponding natural orbitals associated with these resonance states. Table 1 reports the calculated resonance positions and associated widths for the three π^* shape resonance states of the thymine nucleobase, obtained using the cc-pVDZ+2s,2p,2d basis set. The three anionic π^* shape resonances for thymine are observed at 0.69, 2.35, and 5.69 eV respectively. The $1\pi^*$ state has a width of 0.014 eV that corresponds to a lifetime of ~ 47 fs. The $2\pi^*$ resonance state is significantly less stable, with its lifetime reduced to ~ 24 fs. As expected, the $3\pi^*$ resonance appears at a higher energy level of 5.69 eV and is the least stable among the three, with a very short lifetime of around 6 fs. Overall, as the energy of the resonance increases, the states become broader and shorter-lived, indicating stronger coupling with the continuum and faster electron loss.

The shape resonance positions of the $1\pi^*$ and $2\pi^*$ states are in great agreement with the GPA-EA-EOM-CCSD results obtained by Fennimore and Matsika³⁶ (See Table 1). However, the resonance energy of thymine $3\pi^*$ state in this study is overestimated by 0.67 eV. These high-lying shape-resonance states have a strong coupling with the adjacent Feshbach resonance and are more difficult to simulate in a single reference method like EA-EOM-CCSD. The resonance positions of $3\pi^*$ state in our results are underestimated by 0.55 eV when compared with those obtained through the SAC-CI method with complex absorbing potentials, as reported by Sommerfield and Ehara.⁵³ However, the $1\pi^*$ and $2\pi^*$ states are well reproduced. The R-matrix results show wide variation among them, presumably due to the nature of the electronic structure method used.^{68,96}

Our results consistently underestimate the widths of thymine anion shape resonances relative to those reported in previous studies (Table 1). The previously reported values for the width of anionic thymine resonances also show considerable deviation among them, the only general agreement being that the width tends to increase with the resonance energy. Additionally, other available theoretical methods consistently predict relatively large widths for the third shape resonance, typically ranging from 0.4 to 1.0 eV. However, in this study, we obtained a relatively smaller width for the $3\pi^*$ resonance. Unfortunately, there is no experimental data available for the widths of these resonance states. It should be noted that the calculated resonance position and width depend upon three factors, the underlying electronic structure method, the L^2 methods used to calculate complex energy, and the basis set used for the calculations. The

variation of one or more factors can lead to significant differences in widths among different studies using the stabilization approach and the resonance width being a more sensitive property is more prone to variation.

4.2 Adenine shape resonances:

Adenine generally has the lowest electron affinity values among all the nucleobases.⁹⁷ The valence bound anionic states of isolated adenine are neither vertically bound nor adiabatically. The dipole bound states of Adenine are very feebly bound due to its low dipole moment.⁹⁸ Therefore, the valence-bound shape resonance states play an important role in the electron capture process. We have characterized four low-lying π^* shape resonance states associated with the adenine anion nucleobase. The stabilization graph, along with the natural orbitals corresponding to the π^* shape resonance states of adenine, is shown in Figure 1B. The resonance energies and corresponding widths of the adenine shape resonances, along with a comparison to previously reported theoretical and experimental results, are provided in Table 2. The four shape resonances for adenine anion have been identified at 1.11 eV, 1.98 eV, 2.97 eV, and 7.20 eV, respectively. However, only three shape resonances have been identified experimentally in the electron transmission spectroscopy studies conducted by Aflatooni et al.⁹⁵ Our calculated values for the first three resonances differ from the experimental results by approximately 0.5-0.7 eV, similar to that of the thymine. The fourth resonance around 7.20 eV lies outside the experimentally reported range and may not have been observed due to its weak intensity or broad character.

The $1\pi^*$ and $2\pi^*$ shape resonances of adenine anion have relatively narrow widths and correspond to lifetimes of approximately 50 fs and 25 fs, respectively. The third resonance is broader with a width of 0.038 eV and has a much shorter lifetime of around 17 fs. The high-lying $4\pi^*$ resonance is the broadest and most short-lived, with a lifetime of ~ 3 fs. This trend of decreasing lifetimes with an increase in resonance energy suggests stronger interaction with the continuum in high-lying states. The resonance positions of the first three π^* shape resonances of the adenine anion obtained in the present study are in good agreement with the values reported by Fennimore and Matsika,³⁶ who employed the analytically continued GPA-EA-EOM-CCSD approach. However, the energy of the $4\pi^*$ resonance in our calculations is overestimated by approximately 0.4 eV compared to their results.

The widths of all resonances in our study are underestimated relative to the GPA results, except for the $4\pi^*$ state. These discrepancies may arise not only from methodological differences between the RVP and GPA approaches but also from the potential mixing of the $4\pi^*$ state with the first Feshbach adenine resonances, which makes it more challenging to simulate. Our calculated resonance energies are consistent with those reported by Sommerfeld and Ehara using the SAC-CI method combined with CAP.⁵³ Our results underestimate the widths, although the qualitative trends match the previously reported theoretical data quite well.

4.3 AT base pair (linear):

We have identified seven π^* shape resonances in the AT anion base pair, which are consistent with the sum of resonances observed in the isolated adenine and thymine anionic nucleobases. The stabilization plot for the AT base pair, calculated at the RVP/EA-EOM-DLPNO-CCSD/cc-pVDZ+2s2p2d level of theory, is shown in Figure 3B. To confirm the nature of the resonances in the AT base pair, we analyzed the natural orbitals corresponding to the stabilized region in the plot. Figure 2 shows the natural orbitals of the seven π^* shape resonances identified for the AT base pair anion, along with a comparison to the natural orbitals of the corresponding anionic resonances in isolated adenine and thymine. Among these, the lowest lying $1\pi^*$ resonance is located at 0.67 eV with a width of 0.011 eV, while the highest $7\pi^*$ resonance appears at 6.80 eV with a width of 0.116 eV, illustrating the wide range of resonance positions and lifetimes generated by base pairing.

We further compared the resonance energies and widths of the AT base pair anion with those of the individual adenine and thymine anions to assess the effect of base pairing on the resonance parameters. Table 3 summarizes the resonance energy positions and widths determined for the shape resonance states of Thymine, Adenine, and AT base pair calculated at the RVP-EA-EOM-DLPNO-CCSD/cc-pVDZ+2s2p2d level of theory. The reported values for resonance energy and width are from the well-behaved, statistically stable region for each resonance state. The comparison reveals that the $1\pi^*$, $4\pi^*$, and $6\pi^*$ shape resonances of the AT base pair are similar in nature to the thymine resonances, while the $2\pi^*$, $3\pi^*$, $5\pi^*$, and $7\pi^*$ resonances resemble those of adenine. This correspondence is evident both in the character of the resonance states and in the associated energies and widths. The natural orbitals associated with the lowest four π^* resonances of the AT anion show considerable delocalization of electron density over both nucleobases (Figure 2). This suggests that interactions between the low-lying

orbitals of adenine and thymine contribute to the formation of distinct anionic states, with electron density preferentially localized on one base or the other.

While simulating the TNIs of AT base pair, we observe significant interactions between the resonance states of adenine and thymine. As evident from Figure 2, AT-1 π^* resonance is thymine centered with an energy of 0.67 eV. It is slightly stabilized compared to the corresponding thymine 1 π^* , which has an energy of 0.69 eV. Moreover, it also has a contribution from the 1 π^* resonance of adenine which becomes clear in the natural orbital plot. The second AT-2 π^* state is primarily adenine-centered with an energy of 1.26 eV and shows contribution from thymine 1 π^* state. It is destabilized by the 0.15 eV compared to the corresponding adenine 1 π^* resonance at 1.11 eV. Similarly, the adenine-centered AT-3 π^* resonance, which is similar to adenine 2 π^* state, also has a contribution from thymine. AT-3 π^* state is also energetically stabilized by 0.05 eV compared to its corresponding adenine 2 π^* shape resonance. The AT-4 π^* resonance is thymine-centered and is located at 2.43 eV, and its natural orbital plot is similar to the thymine 2 π^* state, but with slight contribution from adenine orbital state. This state is destabilized by 0.08 eV relative to the isolated thymine 2 π^* resonance.

For the higher-lying resonances, the AT-5 π^* shape resonance is largely localized on the adenine nucleobase. Although it is similar to 3 π^* states of Adenine, AT-5 π^* also has contribution from thymine. The subsequent 6 π^* and 7 π^* resonances in AT anion are primarily thymine and adenine centered, respectively. The trends observed in AT base pair show contrast to those observed in GC base pair in two respects. First all the low-lying resonances observed in adenine and thymine are identifiable in AT base pair. Although their positions got shifted there is no qualitative change in their character. On the contrary in GC base pair the guanine centered 1 π^* was not observed. Secondly, in case of GC all the purine centered resonances were blue shifted, and pyrimidine centered resonances are redshifted. On the contrary, the 2 π^* state of thymine (4 π^* states in AT) gets blue shifted, and the 2 π^* and 4 π^* states of adenine (3 π^* and 7 π^* in AT) got red shifted.

The resonances of the base pair follow the same trend as the individual nucleobase resonances. The state that is red shifted shows a reduction in the width on going from nucleobase to base pair, indicating a longer lifetime. On the other hand, there is an increase in the resonance width of the states which has undergone a blueshift. The change in the resonance state from isolated molecules to aggregates; we observe that, for several resonances, the widths decrease when going from the nucleobase anions to the AT base pair, indicating longer lifetimes. However,

some states show an increase in width. These results suggest that while the proximity of the nucleobases can stabilize certain nucleobase-centered resonances and enhance their lifetimes, the effect is state-dependent and does not uniformly affect all resonances or significantly shift their energies.

The trends observed from isolated nucleobases to the AT base pair can arise from several factors including geometric effects, electronic interactions between the bases, and basis set effects.

4.3 Stacking vs base pair effect:

In biological environment, base pairs are stacked on top of other base pairs due to the helical structure of DNA. This stacking leads to π - π interactions between the aromatic rings of adjacent bases, which can significantly influence the stability and decay behavior of resonance states. To assess the impact of stacking on the AT base pair, we have performed resonance calculations for the stacked AT conformation (sAT) and compared the results with those obtained for the linear geometry. We have identified seven π^* resonances associated with the sAT anion base pair, mimicking their native arrangement in the DNA double helix. The stabilization plot for sAT anion base pair is present in Figure 3A.

Table 4 summarizes the resonance parameters of the AT base pair anion resonances in the stacked and linear conformations. The lowest-lying sAT- $1\pi^*$ resonance exhibits a small decrease in energy relative to the corresponding state in the AT base pair, with its resonance position and width are red shifted by 0.03 eV and 0.002 eV respectively. The sAT- $2\pi^*$ state has an energy of 0.88 eV with a lifetime of 47 fs. This represents an increase in stabilization of about 6 fs compared to the corresponding state in the AT- $2\pi^*$ and the resonance position got red-shifted by 0.38 eV. The same trend is observable for the higher resonance states in sAT where all the resonance position and their width got red shifted with respect to the AT base pair. This is presumably due to head-on overlap of π^* orbital in sAT which results in better delocalization of the extra negative charge than that provided by side-on overlap in linear AT base pair, resulting in more stable and long-lived resonance states in the former. All the resonance states in sAT are red shifted as compared to their position and width in isolated nucleobase. The redshift in position with respect to isolated nucleobase varies widely from state to state. It can be as small 0.05 eV in $1\pi^*$ to 0.7 eV in $7\pi^*$ states. It shows that stacked AT can act as an electron sink in larger DNA strands.

4.4 The effect of base-sequence:

Experimentally it has been observed that the base sequence plays an important role in determining the extent of electron attachment induced damage.⁹⁹ We examined the stacked AA and TT base pairs to provide more insight into the role of base sequence in modulating the electronic and structural properties of anionic resonances in DNA. This allows one to study the contributions of homobases stacking, thereby providing a broader perspective on how stacking influences the stability of the resonance states. The stabilization graphs corresponding to stacked AA and TT base pairs are provided in Figure S2.

We have identified eight π^* shape resonances in the stacked AA anion system, which is twice the number observed for the isolated adenine nucleobase. The natural orbitals associated with the resonance states are shown in Figure 5. This increase in the number of resonances arises from the interaction between the two adenine bases, leading to orbital coupling and the formation of delocalized π^* states across the dimer. Similar behavior is observed for thymine for which we have identified six π^* resonances (Figure 6). In both cases, a particular π^* resonances of two nucleobases interact, which leads to stabilization of one and destabilization of the other. The resonance states which got redshifted with respect to their position in the individual base also shows redshift in their resonance width. On the other hand, the resonance states whose position has undergone blueshift their lifetime also decreases with stacking. The stabilization observed due to stacking in sTT and sAA is much smaller than that observed in sAT.

5. Conclusions

In this work, we have examined how base pairing and π - π stacking interactions affect the nature of electron attachment induced resonance states in AT base pairs in DNA. We have identified total seven π^* type shape resonance states in AT base pair. Three of them are thymine centered and four of them are adenine centered. Our analysis shows that the base pairing does not change the qualitative nature of the resonance from that observed in isolated base pair. However, the base pairing significantly affects the stability of the resonances. The first, third and sixth resonance states got stabilized with respect to the corresponding states in isolated nucleobase with their resonance position and width undergoing redshift. The rest of the four resonance states undergo blueshift in position and width. The resonance states in AT which has undergone redshift (and blueshift) contains both pyrimidine and purine centered resonances, which is in sharp contrast to the resonances observed in GC base pair. All the low-lying pyrimidine-

centered resonances in GC have shown to undergo redshift and the purine-centered resonances undergone blueshift.

The stacked AT has been to be an effective sink for electrons, where all the seven resonance states undergo redshift. The redshift in resonance position and width stacked AT is much larger than that observed in the linear base pairs. The lower energy and higher lifetime allow the possibility of formation of stable valence bound state due to geometric relaxation, which may make AT stacked less prone to strand breaking and more prone to base damage.⁴ The TT and AA stacked sequence are less effective as an electron sink as the stability observed due to stacking is much less than that observed in AT base pair.

It will be interesting to study the effect of base pair and stacking on anionic resonances in DNA using more realistic models with sugar and phosphate backbone. Work is in progress towards that direction.

Supplementary material: The optimized geometries of isolated nucleobases, base-pair and stacked nucleobases, additional stabilization plots are provided in the supporting information.

Acknowledgments

The authors acknowledge the support from the IIT Bombay, UGC-India, Prime Minister's Research Fellowship, for financial support. IIT Bombay super computational facility, and C-DAC Supercomputing resources (Param Smriti, Param Brahma) for computational time AKD acknowledges the research fellowship funded by the EU NextGenerationEU through the Recovery and Resilience Plan for Slovakia under project No. 09I03-03-V04-00117.

References:

- (1) Rezaee, M.; Adhikary, A. The Effects of Particle LET and Fluence on the Complexity and Frequency of Clustered DNA Damage. *DNA* **2024**, *4* (1), 34–51.
- (2) O'Neill, P. Radiation-Induced Damage in DNA. In *Studies in Physical and Theoretical Chemistry*; Jonah, C. D., Rao, B. S. M., Eds.; Radiation Chemistry; Elsevier, 2001; Vol. 87, pp 585–622.
- (3) Alizadeh, E.; Sanche, L. Precursors of Solvated Electrons in Radiobiological Physics and Chemistry. *Chem. Rev.* **2012**, *112* (11), 5578–5602.
- (4) Narayanan S J, J.; Tripathi, D.; Dutta, A. K. Doorway Mechanism for Electron Attachment Induced DNA Strand Breaks. *J. Phys. Chem. Lett.* **2021**, *12* (42), 10380–10387.
- (5) Narayanan S J, J.; Tripathi, D.; Verma, P.; Adhikary, A.; Dutta, A. K. Secondary Electron Attachment-Induced Radiation Damage to Genetic Materials. *ACS Omega* **2023**, *8* (12), 10669–10689.
- (6) Cadet, J.; Bellon, S.; Douki, T.; Frelon, S.; Gasparutto, D.; Muller, E.; Pouget, J.-P.; Ravanat, J.-L.; Romieu, A.; Sauvaigo, S. Radiation-Induced DNA Damage: Formation, Measurement, and Biochemical Features. **2004**, *23* (1), 12.
- (7) Berthel, E.; Ferlazzo, M. L.; Devic, C.; Bourguignon, M.; Foray, N. What Does the History of Research on the Repair of DNA Double-Strand Breaks Tell Us?—A Comprehensive Review of Human Radiosensitivity. *Int. J. Mol. Sci.* **2019**, *20* (21).
- (8) Obodovskiy, I. Radiation Therapy. In *Radiation*; Elsevier, 2019; pp 387–396.
- (9) *DNA Damage, DNA Repair and Disease: Volume 1*; Dizdaroglu, M., Lloyd, R. S., Dizdaroglu, M., LLoyd, R. S., Eds.; The Royal Society of Chemistry, 2020.
- (10) *DNA Damage, DNA Repair and Disease: Volume 2*; Dizdaroglu, M., Lloyd, R. S., Dizdaroglu, M., LLoyd, R. S., Eds.; The Royal Society of Chemistry, 2020.
- (11) Becker, D.; Kumar, A.; Adhikary, A.; Sevilla, M. D. Gamma- and Ion-Beam DNA Radiation Damage: Theory and Experiment. **2020**, 426–457.
- (12) Pimblott, S. M.; LaVerne, J. A. Production of Low-Energy Electrons by Ionizing Radiation. *Proc. 11th Tihany Symp. Radiat. Chem.* **2007**, *76* (8), 1244–1247.
- (13) Herbert, J. M.; Coons, M. P. The Hydrated Electron. *Annu. Rev. Phys. Chem.* **2017**, *68* (1), 447–472.
- (14) Walker, D. C. The Hydrated Electron. *Q. Rev. Chem. Soc.* **1967**, *21* (1), 79–108.

- (15) Steenken, S. Purine Bases, Nucleosides, and Nucleotides: Aqueous Solution Redox Chemistry and Transformation Reactions of Their Radical Cations and E^- and OH Adducts. *Chem. Rev.* **1989**, *89* (3), 503–520.
- (16) Kumar, A.; Sevilla, M. D. Low-Energy Electron (LEE)-Induced DNA Damage: Theoretical Approaches to Modeling Experiment. In *Handbook of Computational Chemistry*; Leszczynski, J., Ed.; Springer Netherlands: Dordrecht, 2012; pp 1215–1256.
- (17) Ma, J.; Kumar, A.; Muroya, Y.; Yamashita, S.; Sakurai, T.; Denisov, S. A.; Sevilla, M. D.; Adhikary, A.; Seki, S.; Mostafavi, M. Observation of Dissociative Quasi-Free Electron Attachment to Nucleoside via Excited Anion Radical in Solution. *Nat. Commun.* **2019**, *10* (1), 102.
- (18) Cobut, V.; Frongillo, Y.; Patau, J. P.; Goulet, T.; Fraser, M.-J.; Jay-Gerin, J.-P. Monte Carlo Simulation of Fast Electron and Proton Tracks in Liquid Water – I. Physical and Physicochemical Aspects. *Radiat. Phys. Chem.* **1998**, *51*, 229–243.
- (19) Kumar, A.; Sevilla, M. D.; Sanche, L. How a Single 5 eV Electron Can Induce Double-Strand Breaks in DNA: A Time-Dependent Density Functional Theory Study. *J. Phys. Chem. B* **2024**, *128* (17), 4053–4062.
- (20) Pluhařová, E.; Schroeder, C.; Seidel, R.; Bradforth, S. E.; Winter, B.; Faubel, M.; Slavíček, P.; Jungwirth, P. Unexpectedly Small Effect of the DNA Environment on Vertical Ionization Energies of Aqueous Nucleobases. *J. Phys. Chem. Lett.* **2013**, *4* (21), 3766–3769.
- (21) Pluhařová, E.; Slavíček, P.; Jungwirth, P. Modeling Photoionization of Aqueous DNA and Its Components. *Acc. Chem. Res.* **2015**, *48* (5), 1209–1217.
- (22) Woldhuis, J.; Verberne, J. B.; Lafleur, M. V. M.; Retèl, J.; Blok, J.; Loman, H. γ -Rays Inactivate ϕ X174 DNA in Frozen Anoxic Solutions at -20°C Mainly by Reactions of Dry Electrons. *Int. J. Radiat. Biol. Relat. Stud. Phys. Chem. Med.* **1984**, *46* (4), 329–330.
- (23) Boudaïffa, B.; Cloutier, P.; Hunting, D.; Huels, M. A.; Sanche, L. Resonant Formation of DNA Strand Breaks by Low-Energy (3 to 20 eV) Electrons. *Science* **2000**, *287* (5458), 1658–1660.
- (24) Fabrikant, I. I.; Eden, S.; Mason, N. J.; Fedor, J. *Recent Progress in Dissociative Electron Attachment: From Diatomics to Biomolecules*, 1st ed.; Elsevier Inc., 2017; Vol. 66.
- (25) Pan, X.; Cloutier, P.; Hunting, D.; Sanche, L. Dissociative Electron Attachment to DNA. *Phys. Rev. Lett.* **2003**, *90* (20), 208102.

- (26) Wang, X.-D.; Xuan, C.-J.; Feng, W.-L.; Tian, S. X. Dissociative Electron Attachments to Ethanol and Acetaldehyde: A Combined Experimental and Simulation Study. *J. Chem. Phys.* **2015**, *142* (6), 064316.
- (27) Ptasinska, S. A Missing Puzzle in Dissociative Electron Attachment to Biomolecules: The Detection of Radicals. *Atoms* **2021**, *9* (4).
- (28) Bald, I.; Čurík, R.; Kopyra, J.; Tarana, M. Dissociative Electron Attachment to Biomolecules. In *Nanoscale Insights into Ion-Beam Cancer Therapy*; Solov'yov, A. V., Ed.; Springer International Publishing: Cham, 2017; pp 159–207.
- (29) Kopyra, J. Low Energy Electron Attachment to the Nucleotide Deoxycytidine Monophosphate: Direct Evidence for the Molecular Mechanisms of Electron-Induced DNA Strand Breaks. *Phys. Chem. Chem. Phys.* **2012**, *14* (23), 8287–8289.
- (30) Sanche, L. Low Energy Electron-Driven Damage in Biomolecules. *Eur. Phys. J. D* **2005**, *35* (2), 367–390.
- (31) Gu, J.; Wang, J.; Leszczynski, J. Electron Attachment-Induced DNA Single Strand Breaks: C3'- O3' σ -Bond Breaking of Pyrimidine Nucleotides Predominates. *J. Am. Chem. Soc.* **2006**, *128* (29), 9322–9323.
- (32) Kumari, B.; Huwaidi, A.; Robert, G.; Cloutier, P.; Bass, A. D.; Sanche, L.; Wagner, J. R. Shape Resonances in DNA: Nucleobase Release, Reduction, and Dideoxynucleoside Products Induced by 1.3 to 2.3 eV Electrons. *J. Phys. Chem. B* **2022**, *126* (28), 5175–5184.
- (33) Mukherjee, M.; Ragesh Kumar, T. P.; Ranković, M.; Nag, P.; Fedor, J.; Krylov, A. I. Spectroscopic Signatures of States in the Continuum Characterized by a Joint Experimental and Theoretical Study of Pyrrole. *J. Chem. Phys.* **2022**, *157* (20), 204305.
- (34) Sieradzka, A.; Gorfinkiel, J. D. Theoretical Study of Resonance Formation in Microhydrated Molecules. II. Thymine-(H₂O)_n, n = 1,2,3,5. *J. Chem. Phys.* **2017**, *147* (3), 034303–034303.
- (35) Fennimore, M. A.; Matsika, S. Core-Excited and Shape Resonances of Uracil. *Phys. Chem. Chem. Phys.* **2016**, *18* (44), 30536–30545.
- (36) Fennimore, M. A.; Matsika, S. Electronic Resonances of Nucleobases Using Stabilization Methods. *J. Phys. Chem. A* **2018**, *122* (16), 4048–4057.
- (37) Slaughter, D. S.; Rescigno, T. N. Breaking up Is Hard to Do. *Nat. Phys.* **2018**, *14* (2), 109–110.
- (38) Ji, J.-B.; Guo, Z.; Driver, T.; Trevisan, C. S.; Cesar, D.; Cheng, X.; Duris, J.; Franz, P. L.; Glownia, J.; Gong, X.; Hammerland, D.; Han, M.; Heck, S.; Hoffmann, M.; Kamalov,

- A.; Larsen, K. A.; Li, X.; Lin, M.-F.; Liu, Y.; McCurdy, C. W.; Obaid, R.; O'Neal, J. T.; Rescigno, T. N.; Robles, R. R.; Sudar, N.; Walter, P.; Wang, A. L.; Wang, J.; Wolf, T. J. A.; Zhang, Z.; Ueda, K.; Lucchese, R. R.; Marinelli, A.; Cryan, J. P.; Wörner, H. J. Attosecond X-Ray Core-Level Chronoscopy of Aromatic Molecules. *Phys. Rev. X* **2025**, *15* (4), 041031.
- (39) Nisoli, M.; Decleva, P.; Calegari, F.; Palacios, A.; Martín, F. Attosecond Electron Dynamics in Molecules. *Chem. Rev.* **2017**, *117* (16), 10760–10825.
- (40) Barrios, R.; Skurski, P.; Simons, J. Mechanism for Damage to DNA by Low-Energy Electrons. *J. Phys. Chem. B* **2002**, *106* (33), 7991–7994.
- (41) Bryjko, L.; Mourik, T. van; Dora, A.; Tennyson, J. R-Matrix Calculation of Low-Energy Electron Collisions with Phosphoric Acid. *J. Phys. B At. Mol. Opt. Phys.* **2010**, *43*, 235203.
- (42) Winstead, C.; McKoy, V. Low-Energy Electron Collisions with Gas-Phase Uracil. *J. Chem. Phys.* **2006**, *125* (17), 174304–174304.
- (43) Li, X.; Sevilla, M. D.; Sanche, L. Density Functional Theory Studies of Electron Interaction with DNA: Can Zero eV Electrons Induce Strand Breaks? *J. Am. Chem. Soc.* **2003**, *125* (45), 13668–13669.
- (44) Verma, P.; Narayanan S J, J.; Dutta, A. K. Electron Attachment to DNA: The Protective Role of Amino Acids. *J. Phys. Chem. A* **2023**, *127* (10), 2215–2227.
- (45) Verma, P.; Mukherjee, M.; Bhattacharya, D.; Haritan, I.; Dutta, A. K. Shape Resonance Induced Electron Attachment to Cytosine: The Effect of Aqueous Media. *J. Chem. Phys.* **2023**, *159* (21), 214303.
- (46) Martin, F.; Burrow, P. D.; Cai, Z.; Cloutier, P.; Hunting, D.; Sanche, L. DNA Strand Breaks Induced by 0-4 eV Electrons: The Role of Shape Resonances. *Phys. Rev. Lett.* **2004**, *93* (6), 6–9.
- (47) Moiseyev, N. *Non-Hermitian Quantum Mechanics*; Cambridge University Press, 2011.
- (48) Rescigno, T. N.; McCurdy, C. W.; Orel, A. E. Extensions of the Complex-Coordinate Method to the Study of Resonances in Many-Electron Systems. *Phys. Rev. A* **1978**, *17*, 1931–1938.
- (49) Hernández Vera, M.; Jagau, T.-C. Resolution-of-the-Identity Second-Order Møller–Plesset Perturbation Theory with Complex Basis Functions: Benchmark Calculations and Applications to Strong-Field Ionization of Polyacenes. *J. Chem. Phys.* **2020**, *152* (17), 174103.

- (50) White, A. F.; Epifanovsky, E.; McCurdy, C. W.; Head-Gordon, M. Second Order Møller-Plesset and Coupled Cluster Singles and Doubles Methods with Complex Basis Functions for Resonances in Electron-Molecule Scattering. *J. Chem. Phys.* **2017**, *146* (23), 234107.
- (51) Moiseyev, N.; Corcoran, C. Autoionizing States of H₂ and H₂⁻ Using the Complex-Scaling Method. *Phys Rev A* **1979**, *20* (3), 814–817.
- (52) Jagau, T. C.; Bravaya, K. B.; Krylov, A. I. Extending Quantum Chemistry of Bound States to Electronic Resonances. *Annu. Rev. Phys. Chem.* **2017**, *68*, 525–553.
- (53) Kanazawa, Y.; Ehara, M.; Sommerfeld, T. Low-Lying Π^* Resonances of Standard and Rare DNA and RNA Bases Studied by the Projected CAP/SAC-CI Method. *J. Phys. Chem. A* **2016**, *120* (9), 1545–1553.
- (54) Sajeev, Y.; Ghosh, A.; Vaval, N.; Pal, S. Coupled Cluster Methods for Autoionisation Resonances. *Int. Rev. Phys. Chem.* **2014**, *33* (3), 397–425.
- (55) Jagau, T.-C.; Zuev, D.; Bravaya, K. B.; Epifanovsky, E.; Krylov, A. I. A Fresh Look at Resonances and Complex Absorbing Potentials: Density Matrix-Based Approach. *J. Phys. Chem. Lett.* **2014**, *5* (2), 310–315.
- (56) Sajeev, Y.; Moiseyev, N. Reflection-Free Complex Absorbing Potential for Electronic Structure Calculations: Feshbach-Type Autoionization Resonances of Molecules. *J. Chem. Phys.* **2007**, *127* (3), 034105.
- (57) Sommerfeld, T.; Ehara, M. Complex Absorbing Potentials with Voronoi Isosurfaces Wrapping Perfectly around Molecules. *J. Chem. Theory Comput.* **2015**, *11* (10), 4627–4633.
- (58) Gayvert, J. R.; Bravaya, K. B. Projected CAP-EOM-CCSD Method for Electronic Resonances. *J. Chem. Phys.* **2022**, *156* (9), 094108.
- (59) Gayvert, J. R.; Bravaya, K. B. Application of Box and Voronoi CAPs for Metastable Electronic States in Molecular Clusters. *J. Phys. Chem. A* **2022**, *126* (30), 5070–5078.
- (60) Das, S.; Samanta, K. Recent Advances in the Study of Negative-Ion Resonances Using Multiconfigurational Propagator and a Complex Absorbing Potential. *ChemPhysChem* **2023**, *24* (3), e202200546.
- (61) Hazi, A. U.; Taylor, H. S. Stabilization Method of Calculating Resonance Energies: Model Problem. *Phys Rev A* **1970**, *1* (4), 1109–1120.
- (62) Landau, A.; Haritan, I.; Moiseyev, N. The RVP Method—From Real Ab-Initio Calculations to Complex Energies and Transition Dipoles. *Front. Phys.* **2022**, *10*.

- (63) Landau, A.; Haritan, I.; Kaprálová-Žd'ánská, P. R.; Moiseyev, N. Atomic and Molecular Complex Resonances from Real Eigenvalues Using Standard (Hermitian) Electronic Structure Calculations. *J. Phys. Chem. A* **2016**, *120* (19), 3098–3108.
- (64) Haritan, I.; Moiseyev, N. On the Calculation of Resonances by Analytic Continuation of Eigenvalues from the Stabilization Graph. *J. Chem. Phys.* **2017**, *147* (1), 014101.
- (65) Abdoul-Carime, H.; Gohlke, S.; Fischbach, E.; Scheike, J.; Illenberger, E. Thymine Excision from DNA by Subexcitation Electrons. *Chem. Phys. Lett.* **2004**, *387* (4–6), 267–270.
- (66) Burrow, P. D.; Gallup, G. A.; Scheer, A. M.; Denifl, S.; Ptasińska, S.; Märk, T.; Scheier, P. Vibrational Feshbach Resonances in Uracil and Thymine. *J. Chem. Phys.* **2006**, *124* (12), 124310–124310.
- (67) Denifl, S.; Ptasińska, S.; Probst, M.; Hrušák, J.; Scheier, P.; Märk, T. D. Electron Attachment to the Gas-Phase DNA Bases Cytosine and Thymine. *J. Phys. Chem. A* **2004**, *108* (31), 6562–6569.
- (68) Dora, A.; Bryjko, L.; Mourik, T. van; Tennyson, J. R-Matrix Study of Elastic and Inelastic Electron Collisions with Cytosine and Thymine. *J. Phys. B At. Mol. Opt. Phys.* **2012**, *45* (17), 175203.
- (69) Berdys, J.; Skurski, P.; Simons, J. Damage to Model DNA Fragments by 0.25-1.0 eV Electrons Attached to a Thymine Π^* Orbital. **2004**.
- (70) McAllister, M.; Kazemigazestane, N.; Henry, L. T.; Gu, B.; Fabrikant, I.; Tribello, G. A.; Kohanoff, J. Solvation Effects on Dissociative Electron Attachment to Thymine. *J. Phys. Chem. B* **2019**, *123* (7), 1537–1544.
- (71) Bouskila, G.; Landau, A.; Haritan, I.; Moiseyev, N.; Bhattacharya, D. Complex Energies and Transition Dipoles for Shape-Type Resonances of Uracil Anion from Stabilization Curves via Padé. *J. Chem. Phys.* **2022**, *156* (19), 194101.
- (72) Cheng, H.-Y.; Chen, C.-W. Energy and Lifetime of Temporary Anion States of Uracil by Stabilization Method. *J. Phys. Chem. A* **2011**, *115* (35), 10113–10121.
- (73) Cooper, G.; Clarke, C.; Verlet, J. Electron Impact Resonances of Uracil in an Aqueous Environment from Anion Photoelectron Imaging. *J. Phys. B At. Mol. Opt. Phys.* **2023**, *56*.
- (74) Verma, P.; Ghosh, D.; Dutta, A. K. Electron Attachment to Cytosine: The Role of Water. *J. Phys. Chem. A* **2021**, *125* (22), 4683–4694.

- (75) Bhaskaran, R.; Sarma, M. Low Energy Electron Induced Cytosine Base Release in 2'-Deoxycytidine-3'-Monophosphate via Glycosidic Bond Cleavage: A Time-Dependent Wavepacket Study. *J. Chem. Phys.* **2014**, *141* (10), 104309–104309.
- (76) Arora, S.; Narayanan, S. J. J.; Dutta, A. K. How Good Is the Time-Dependent DFT Method for Simulating Anionic Shape Resonances of DNA Nucleobases? *J. Chem. Sci.* **2025**, *137* (4), 119.
- (77) Tripathi, D.; Pyla, M.; Dutta, A. K.; Matsika, S. Impact of Solvation on the Electronic Resonances in Uracil. *Phys. Chem. Chem. Phys.* **2025**, *27* (7), 3588–3601.
- (78) Pyla, M.; Matsika, S. Partial Widths of Shape Resonances in Pyridine and Uracil Using the Stabilization Method. *J. Chem. Phys.* **2026**, *164* (1), 014308.
- (79) Narayanan S J, J.; Tripathi, D.; Haritan, I.; Dutta, A. K. The Effect of Aqueous Medium on Nucleobase Shape Resonances: Insights from Microsolvation. *J. Phys. Chem. A* **2025**, *129* (48), 11179–11188.
- (80) Colson, A. O.; Besler, B.; Sevilla, M. D. Ab Initio Molecular Orbital Calculations on DNA Base Pair Radical Ions: Effect of Base Pairing on Proton-Transfer Energies, Electron Affinities, and Ionization Potentials. *J. Phys. Chem.* **1992**, *96* (24), 9787–9794.
- (81) Al-Jihad, I.; Smets, J.; Adamowicz, L. Covalent Anion of the Canonical Adenine–Thymine Base Pair. Ab Initio Study. *J. Phys. Chem. A* **2000**, *104* (13), 2994–2998.
- (82) Smets, J.; Jalbout, A. F.; Adamowicz, L. Anions of the Hydrogen-Bonded Guanine–Cytosine Dimer – Theoretical Study. *Chem. Phys. Lett.* **2001**, *342* (3), 342–346.
- (83) Weigend, F.; Häser, M. RI-MP2: First Derivatives and Global Consistency. *Theor. Chem. Acc.* **1997**, *97* (1), 331–340.
- (84) Weigend, F.; Häser, M.; Patzelt, H.; Ahlrichs, R. RI-MP2: Optimized Auxiliary Basis Sets and Demonstration of Efficiency. *Chem. Phys. Lett.* **1998**, *294* (1), 143–152.
- (85) Weigend, F.; Ahlrichs, R. Balanced Basis Sets of Split Valence, Triple Zeta Valence and Quadruple Zeta Valence Quality for H to Rn: Design and Assessment of Accuracy. *Phys. Chem. Chem. Phys.* **2005**, *7* (18), 3297–3305.
- (86) Pracht, P.; Bohle, F.; Grimme, S. Automated Exploration of the Low-Energy Chemical Space with Fast Quantum Chemical Methods. *Phys Chem Chem Phys* **2020**, *22* (14), 7169–7192.
- (87) Riplinger, C.; Neese, F. An Efficient and near Linear Scaling Pair Natural Orbital Based Local Coupled Cluster Method. *J. Chem. Phys.* **2013**, *138* (3), 034106–034106.

- (88) Dutta, A. K.; Saitow, M.; Demoulin, B.; Neese, F.; Izsák, R. A Domain-Based Local Pair Natural Orbital Implementation of the Equation of Motion Coupled Cluster Method for Electron Attached States. *J. Chem. Phys.* **2019**, *150* (16), 164123.
- (89) Dunning, T. H. Gaussian Basis Sets for Use in Correlated Molecular Calculations. I. The Atoms Boron through Neon and Hydrogen. *J. Chem. Phys.* **1989**, *90* (2), 1007–1023.
- (90) Stoychev, G. L.; Auer, A. A.; Neese, F. Automatic Generation of Auxiliary Basis Sets. *J. Chem. Theory Comput.* **2017**, *13* (2), 554–562.
- (91) Neese, F. The ORCA Program System. *Wiley Interdiscip. Rev. Comput. Mol. Sci.* **2012**, *2* (1), 73–78.
- (92) Neese, F. Software Update: The ORCA Program System—Version 5.0. *WIREs Comput. Mol. Sci.* **2022**, *12* (5), e1606.
- (93) Safrai, Y.; Haritan, I. Automatic-Rvp: RVP Program, 2021. <https://pypi.org/project/automatic-rvp/> (accessed 2023-08-03).
- (94) Arora, S.; Narayanan S J, J.; Haritan, I.; Adhikary, A.; Dutta, A. K. Effect of Protein Environment on the Shape Resonances of RNA Pyrimidine Nucleobases: Insights from a Model System. *J. Chem. Phys.* **2025**, *163* (13), 134103.
- (95) Aflatooni, K.; Gallup, G. A.; Burrow, P. D. Electron Attachment Energies of the DNA Bases. *J. Phys. Chem. A* **1998**, *102* (31), 6205–6207.
- (96) Tonzani, S.; Greene, C. H. Low-Energy Electron Scattering from DNA and RNA Bases: Shape Resonances and Radiation Damage. *J. Chem. Phys.* **2006**, *124* (5), 054312.
- (97) Dutta, A. K.; Sengupta, T.; Vaval, N.; Pal, S. Electron Attachment to DNA and RNA Nucleobases: An EOMCC Investigation. *Int. J. Quantum Chem.* **2015**, *115* (12), 753–764.
- (98) Tripathi, D.; Dutta, A. K. Bound Anionic States of DNA and RNA Nucleobases: An EOM-CCSD Investigation. *Int. J. Quantum Chem.* **2019**, *119* (9), e25875.
- (99) Li, Z.; Cloutier, P.; Sanche, L.; Wagner, J. R. Low-Energy Electron-Induced DNA Damage: Effect of Base Sequence in Oligonucleotide Trimers. *J. Am. Chem. Soc.* **2010**, *132* (15), 5422–5427.
- (100) Winstead, C.; McKoy, V.; d’Almeida Sanchez, S. Interaction of Low-Energy Electrons with the Pyrimidine Bases and Nucleosides of DNA. *J. Chem. Phys.* **2007**, *127* (8), 085105.
- (101) Dora, A.; Bryjko, L.; van Mourik, T.; Tennyson, J. Low-Energy Electron Scattering with the Purine Bases of DNA/RNA Using the R-Matrix Method. *J. Chem. Phys.* **2012**, *136* (2), 024324.

(102) Winstead, C.; McKoy, V. Interaction of Low-Energy Electrons with the Purine Bases, Nucleosides, and Nucleotides of DNA. *J. Chem. Phys.* **2006**, *125* (24), 244302.

Tables and figures:

Table 1: *The comparison of resonance position energies and widths (in parentheses) of Thymine with previous experimental and theoretical results. All values are in eV.*

Thymine	Er(Γ) (eV)		
	$1\pi^*$	$2\pi^*$	$3\pi^*$
RVP/EA-EOM-DLPNO-CCSD (This work)	0.69(0.014)	2.35(0.028)	5.69(0.102)
GPA/EOM-EA-CCSD ³⁶	0.68(0.02)	2.32(0.073)	5.02(0.58)
CAP/SAC-CI ⁵³	0.67(0.11)	2.28(0.15)	5.14(0.41)
R-matrix/u-CC ⁶⁸	0.53(0.08)	2.41(0.10)	5.26
R-matrix/SEP ⁶⁸	0.60(0.11)	2.73(0.11)	5.52(0.57)
SMC/SEP ¹⁰⁰	0.30	0.19	5.70
R-matrix/SE ⁹⁶	2.40(0.20)	5.50(0.60)	7.90(1.00)
Expt. ⁹⁵	0.29	1.71	4.05

Table 2: *The comparison of resonance position energies and widths (in parentheses) of Adenine with previous experimental and theoretical results. Values are given in eV.*

Adenine	Er(Γ) (eV)			
	$1\pi^*$	$2\pi^*$	$3\pi^*$	$4\pi^*$
RVP/EA-EOM-DLPNO-CCSD (This work)	1.11(0.013)	1.98(0.026)	2.97(0.038)	7.20(0.204)
GPA/EOM-EA-CCSD ³⁶	1.13(0.04)	2.01(0.05)	2.96(0.14)	6.78(0.21)
CAP/SAC-CI ⁵³	0.89(0.13)	1.93(0.29)	2.72(0.17)	6.65(0.57)
R-matrix/u-CC ¹⁰¹	1.58(0.22)	2.44(0.14)	4.38(0.67)	7.94(0.57)
R-matrix/SEP ¹⁰¹	1.30(0.14)	2.12(0.09)	3.12(0.28)	7.07(0.24)
SMC/SEP ¹⁰²	1.10	1.80	4.10	
R-matrix/SE ⁹⁶	2.40(0.20)	3.20(0.20)	4.40(0.30)	
Expt. ⁹⁵	0.54	1.36	2.17	

Table 3: The comparison of resonance position energies and widths of **Adenine** and **Thymine** with the **AT** base pair (linear). (The color coding identifies whether an AT resonance is adenine- or thymine-centered, with each assigned the same color as the corresponding isolated nucleobase resonance.)

System	$1\pi^*$	$2\pi^*$	$3\pi^*$	$4\pi^*$	$5\pi^*$	$6\pi^*$	$7\pi^*$
AT	0.67 (0.011)	1.26 (0.016)	1.93 (0.020)	2.43 (0.035)	3.16 (0.044)	5.67 (0.084)	6.80 (0.116)
Adenine	1.11 (0.013)	1.98 (0.026)	2.97 (0.038)	7.20 (0.204)			
Thymine	0.69 (0.014)	2.35 (0.028)	5.71 (0.102)				

Table 4: The comparison of resonance parameters for AT base pair in the stacked and linear geometry.

E _R (Γ) in eV							
System	$1\pi^*$	$2\pi^*$	$3\pi^*$	$4\pi^*$	$5\pi^*$	$6\pi^*$	$7\pi^*$
AT (linear)	0.67 (0.011)	1.26 (0.016)	1.93 (0.020)	2.43 (0.035)	3.16 (0.044)	5.67 (0.084)	6.80 (0.116)
AT (stacked)	0.64 (0.009)	0.88 (0.014)	1.65 (0.016)	2.23 (0.025)	2.73 (0.035)	5.33 (0.071)	6.51 (0.108)

Table 5: The resonance position energies and widths of **AA** and **TT** base pairs.

System	$1\pi^*$	$2\pi^*$	$3\pi^*$	$4\pi^*$	$5\pi^*$	$6\pi^*$	$7\pi^*$	$8\pi^*$
sAA	1.05 (0.012)	1.17 (0.018)	1.92 (0.021)	2.03 (0.033)	2.59 (0.037)	3.16 (0.057)	6.77 (0.127)	7.72 (0.228)
Adenine	1.11 (0.013)	1.98 (0.026)	2.97 (0.038)	7.20 (0.204)				
sTT	0.61 (0.010)	0.73 (0.019)	1.98 (0.024)	2.43 (0.033)	5.42 (0.066)	5.73 (0.110)		
Thymine	0.69 (0.014)	2.35 (0.028)	5.69 (0.102)					

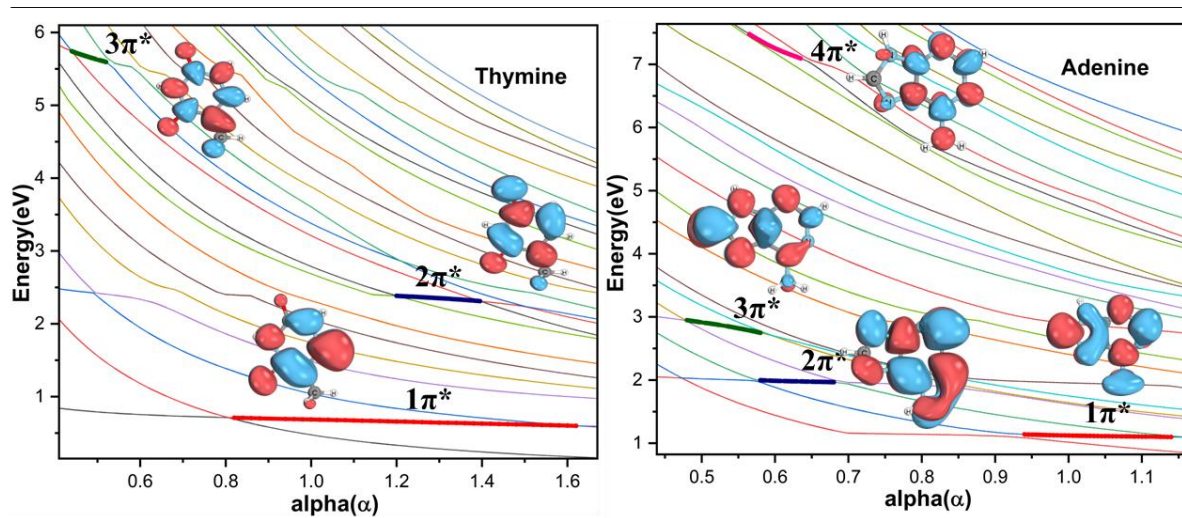
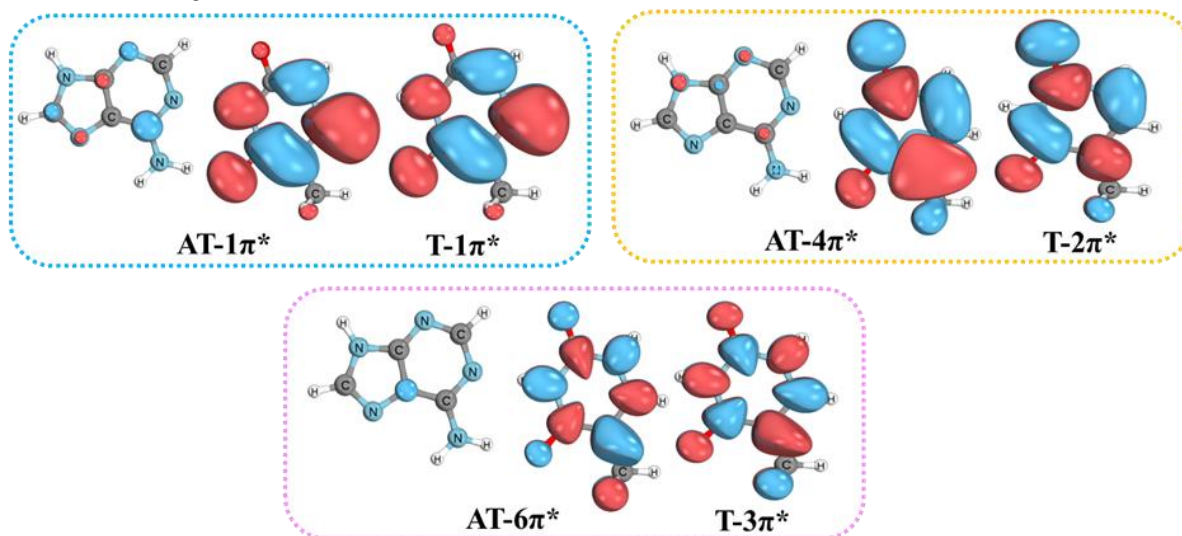


Figure 1: Stabilization plots of A) *Adenine* and B) *Thymine* with the highlighted stable regions and natural orbitals corresponding to the shape resonances.

AT and Thymine



AT and Adenine

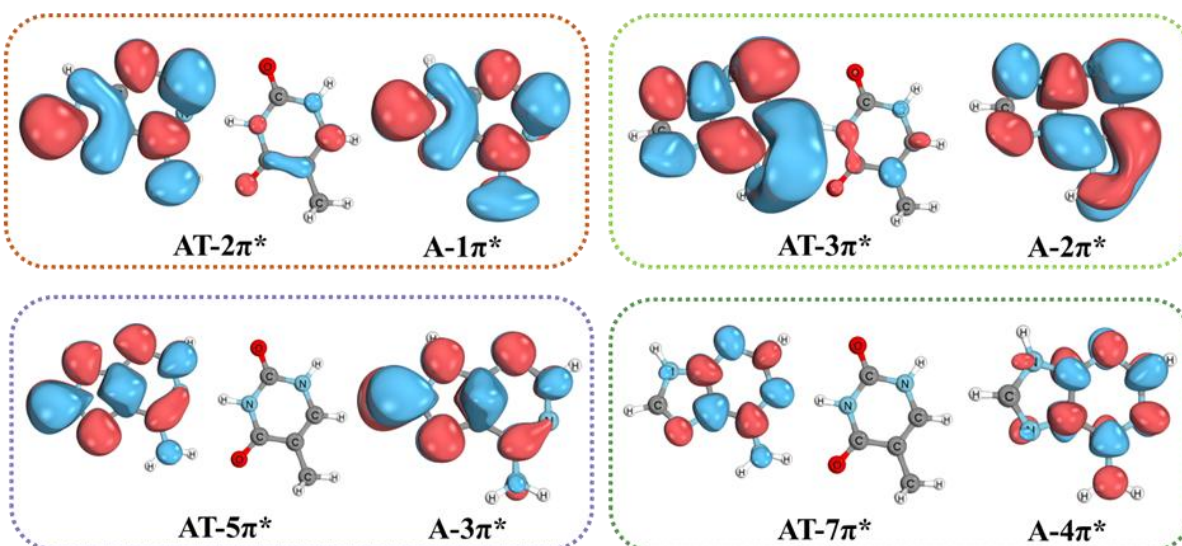


Figure 2: Natural orbitals comparison analysis of adenine and thymine with the AT base pair.

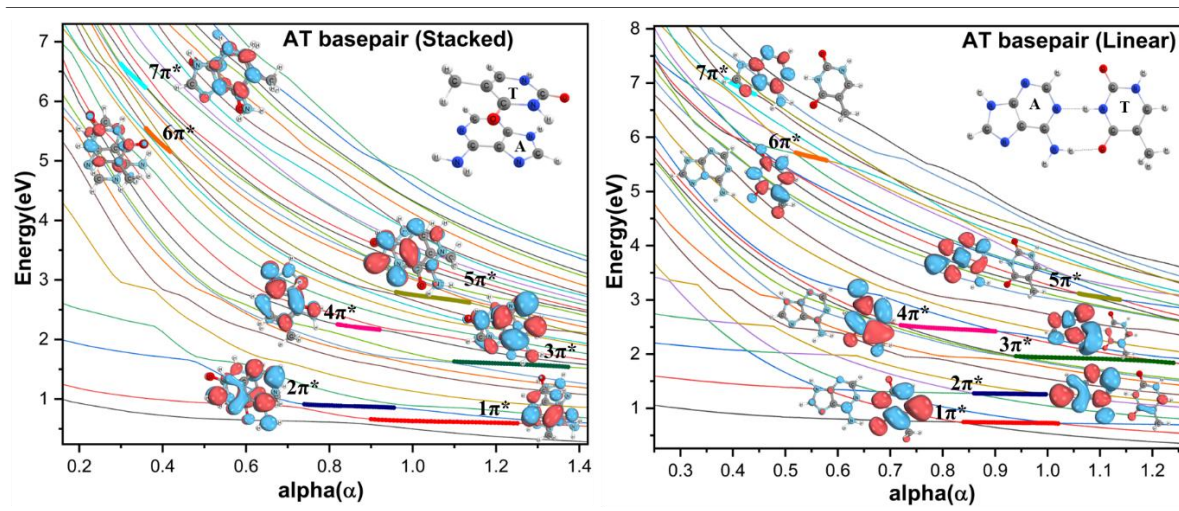


Figure 3: Energy stabilization plots and natural orbitals for A) stacked AT and B) linear AT base pair.

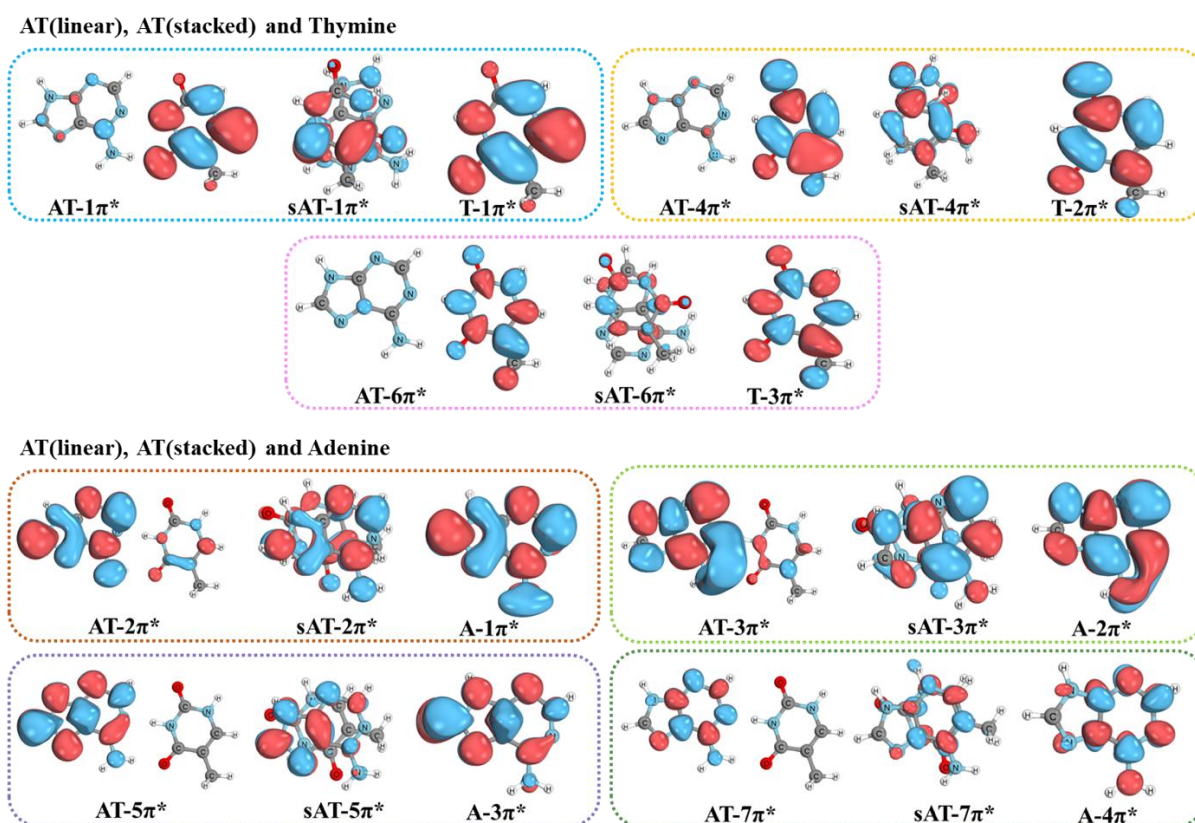


Figure 4: Natural orbitals comparison analysis of isolated adenine and thymine nucleobases with the AT base pair (linear and stacked conformations).

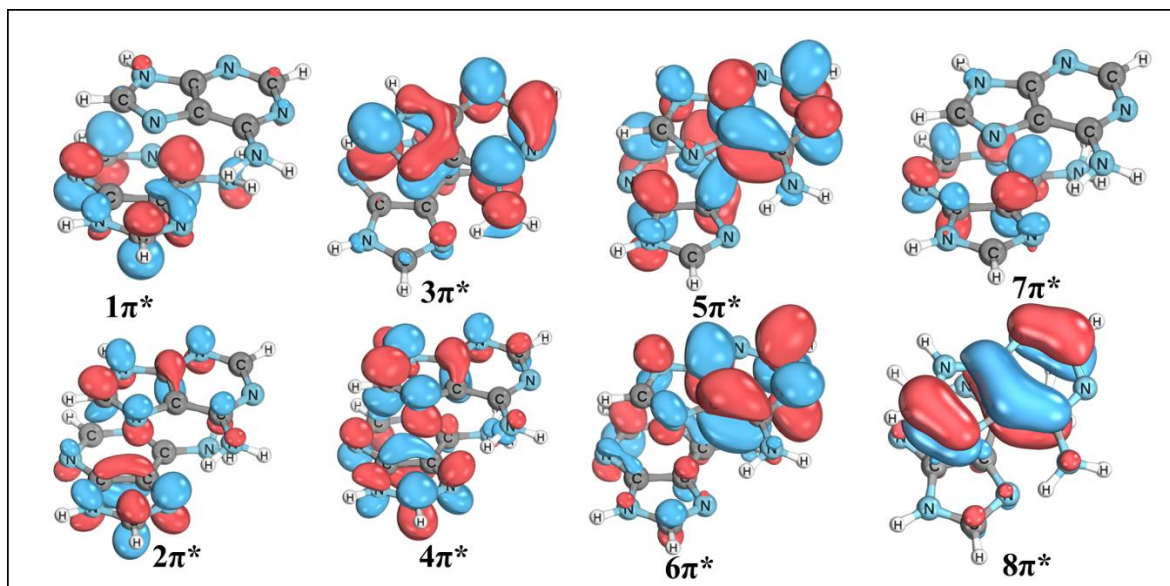


Figure 5: *Natural orbitals corresponding to adenine-adenine stacked base pair.*

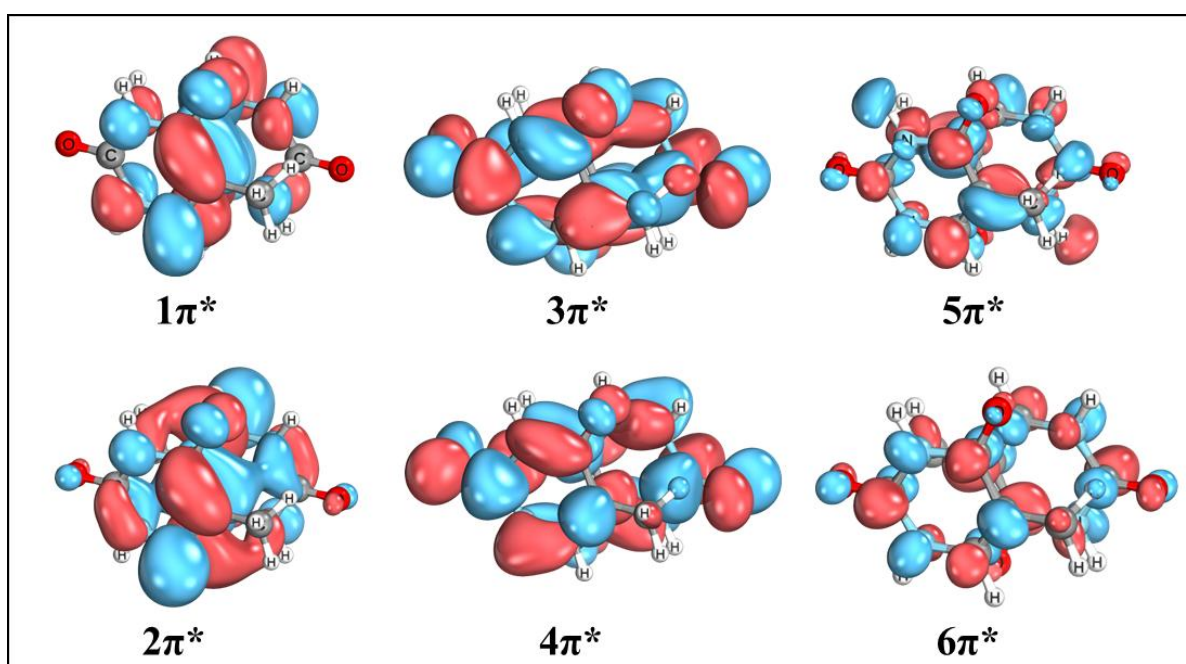


Figure 6: *Natural orbitals corresponding to the thymine-thymine stacked base pair.*